The role of H_2 in Fe carburization by CO in Fischer-Tropsch catalysts

Chai, Jiachun; Pestman, Robert; Chen, Wei; Dugulan, A. Iulian; Feng, Bo; Men, Zhuowu; Wang, Peng; Hensen, Emiel J.M.

DOI
10.1016/j.jcat.2021.05.027

Publication date
2021

Document Version
Final published version

Published in
Journal of Catalysis

Journal of Catalysis 400 (2021) 93–102

Contents lists available at ScienceDirect

Journal of Catalysis

journal homepage: www.elsevier.com/locate/jcat

The role of H_2 in Fe carburization by CO in Fischer-Tropsch catalysts

Jiachun Chai [a], Robert Pestman [a], Wei Chen [a], A. Iulian Dugulan [b], Bo Feng [c], Zhuowu Men [c], Peng Wang [a,c,*], Emiel J.M. Hensen [a,*]

[a] Laboratory of Inorganic Materials Chemistry, Schuit Institute of Catalysis, Department of Chemical Engineering and Chemistry, Eindhoven University of Technology, P.O. Box 513, 5600 MB Eindhoven, the Netherlands
[b] Fundamental Aspects of Materials and Energy Group, Delft University of Technology, 2629 JB Delft, the Netherlands
[c] National Institute of Clean-and-Low-Carbon Energy, Future Science and Technology City, Changping District, Beijing 102211, People's Republic of China

ARTICLE INFO

Article history:
Received 20 April 2021
Revised 25 May 2021
Accepted 26 May 2021
Available online 4 June 2021

Keywords:
Fischer-Tropsch synthesis
Iron
Carburization
Synthesis gas
Mechanism

ABSTRACT

The formation of Fe-carbide phases is relevant to the synthesis of Fischer-Tropsch synthesis catalysts. We investigated the carburization of Raney Fe as a model catalyst using spectroscopic and temperature-programmed techniques. IR spectroscopy shows that CO dissociation already occurs at −150 °C, while C diffusion into metallic Fe requires much higher temperature (~180 °C). The carburization rate increases with increasing H_2/CO ratio, which can be attributed to the lower overall barrier for O removal as H_2O as compared to CO_2. O removal frees vacancies that are needed for CO dissociation. The resulting higher C coverage increases the driving force for Fe-carbide formation. A higher driving force leads to predominant formation of the more carbon-rich ε′()-carbide, while χ-Fe_5C_2 is formed at lower H_2/CO ratio. The removal of surface O appears to be the rate-limiting step under all conditions. Initially, most of deposited C is used for Fe-carbide formation with a small contribution to hydrocarbons formation.

1. Introduction

Fischer-Tropsch (FT) synthesis is an increasingly important technology for producing liquid fuels and chemicals via synthesis gas, which can be obtained from coal, natural gas, or biomass [1,2]. While group 8 and 9 metals show good catalytic activity in FT synthesis, only the most abundant first-row transition metals Fe and Co are used in commercial FT catalysts [3–5]. Fe has several advantages over Co: it is cheaper, can be used in a wider temperature and pressure window, and is more flexible with respect to feedstock composition. Fe is particularly preferred in coal-to-liquids (CTL) processes due to its higher sulfur tolerance and better ability to deal with the low H_2/CO ratio of coal-derived synthesis gas [6].

The active phase of Fe-based FT catalysts comprises Fe-oxides (especially Fe_3O_4), Fe-carbides and metallic Fe [7]. Despite the heterogeneous composition of these catalysts, it has been established that the FT activity correlates strongly with the Fe-carbide content [8]. Therefore, the conversion of the usual Fe-oxide catalyst precursor into the active Fe-carbide form has received widespread attention. ε′()-carbide, χ-Fe_5C_2 and Θ-Fe_3C are typical Fe-carbides active in FT synthesis [9]. The structure of Fe-carbides can be divided into two categories according to the occupation of C atoms in the hexagonally close packed (hcp) Fe lattice [10]. In ε′()-carbide (octahedral carbide), the C atoms are located in the octahedral interstices of the Fe lattice. ε-Fe_2C and ε-$Fe_{2.2}C$ can be distinguished by a slightly different C content. In χ-Fe_5C_2 and Θ-Fe_3C, the C atoms are located in the trigonal prismatic interstices of the Fe lattice. The formation of specific Fe-carbides depends on many factors such as the crystallite size, morphology, surface texture, the presence of promoters (or inhibitors), and the carburization conditions (temperature, pressure and gas composition) [11,12]. De Smit *et al.* studied the stability and interconversion of these Fe-carbide phases as a function of the "carbon chemical potential", which can be linked to the gas-phase composition and the temperature [13]. A higher H_2/CO (lower carbon chemical potential) is predicted to lead to carbon-poor phases such as χ-Fe_5C_2 and Θ-Fe_3C. The methods used to predict these stabilities are rooted in thermodynamics. The stability of the different phases under actual FT conditions will also depend on kinetic factors. Specifically, the diffusion of C atoms derived from CO dissociation from the surface into the bulk of reduced Fe, should be considered. It has been established that the presence of H_2 facilitates carburization, resulting in carbon-richer ε′()-carbide [14].

Most research on Fe carburization has focused on bulk chemical issues in metallurgic context. Generally, the rate of carburization is

* Corresponding authors.
E-mail addresses: peng.wang.hm@chnenergy.com.cn (P. Wang), e.j.m.hensen@tue.nl (E.J.M. Hensen).

https://doi.org/10.1016/j.jcat.2021.05.027
0021-9517/

strongly influenced by the composition of the carburizing gas [15,16]. Fundamental studies often employ high temperature (>500 °C) and iron foil or electrolytic iron as substrates [17], which are not representative for Fe-carbides relevant to the FT reaction. Moreover, the carbon content in steel (typically 0.05–0.35% [18]) is much lower than in Fe-carbide phases in FT catalysts. The unsteady kinetic regimes during carburization make it difficult to correlate bulk carbide formation with the processes and carbon-type intermediates present at the surface. In this context, it is important to develop a better understanding of the carburization mechanism of Fe-based catalysts and, specifically, about the correlation between solid-phase reactions involved in carburization of the bulk of Fe nanoparticles and the catalytic reactions occurring at the surface during carburization.

Mechanistically, Fe-carbide formation involves CO dissociation followed by C diffusion into the bulk as well as C and O removal by surface reactions, regardless whether carburization is applied to metallic Fe or Fe-oxide. A recent previous work showed that careful control of the carburization process of fully reduced Fe leads to pure Fe-carbide [19]. When the Fe precursor is not fully reduced before carburization, it will lead to a mixture of Fe-oxide and Fe-carbides. The remaining Fe-oxide, usually present as hematite (Fe_3O_4), can catalyze the water-gas shift (WGS) reaction, which involves the conversion of CO with H_2O to CO_2 and H_2 [6,7,20]. It should also be noted that the effect of O diffusion can be excluded during the carburization of metallic Fe, as the diffusivity of O atoms into the Fe lattice is much lower than that of C atoms [21]. Hence, the aim of this work is to study the diffusion of C in metallic Fe relevant to Fe carburization.

Mössbauer spectroscopy [22] and X-ray diffraction [23] are the most used techniques to analyze the phase composition of Fe-carbides (and other forms of Fe). These techniques provide only qualitative insight into the actual C content of the phases formed upon carburization [24–26]. In the present work, these two bulk techniques have been complemented with temperature-programmed hydrogenation measurements, allowing to quantitatively determine the amount of C atoms in a carburized Fe samples. IR spectroscopy and XPS are used to investigate the surface composition of such samples in more detail. Especially the impact of H_2 on carburization by CO has been studied using Raney-Fe as a porous and support-free precursor with a reasonable surface area [19], rendering it an ideal model catalyst to investigate the carburization process.

2. Experimental methods

2.1. Catalyst preparation

2.1.1. Raney-Fe catalyst

Raney-Fe was prepared from an aluminum-iron (Al50/Fe50) alloy (Goodfellow, 150 μm powder). A 25 ml 9 M KOH (Sigma-Aldrich) solution was prepared in a round-bottom flask. After heating the solution to 70 °C, 5 g of the Al-Fe alloy powder was slowly added. Caution is needed, as this reaction produces hydrogen. After 40 min of stirring at 70 °C, the mixture was cooled to room temperature. The suspension was washed with water and ethanol 7 times each in order to remove potassium and aluminum hydroxide/oxide ions and retrieve the precipitated Raney-Fe. Due to the pyrophoric character of the fine Fe powder, the catalyst was passivated in a 1% O_2/He flow for 24 h at room temperature for safe handling.

2.1.2. Fe/SiO_2 catalyst

SiO_2-supported Fe sample was prepared by incipient wetness impregnation method of an aqueous solution of $Fe(NO_3)_3{\cdot}9H_2O$ (AR, Sinopharm Chemical Reagent Co.) on a silica support (SiO_2 Q15, 120 mesh, Sasol). The sample was sequentially dried at 80 °C for 12 h and 120 °C for 24 h and then calcined at 500 °C for 5 h in static air [14]. Fe/SiO_2 was used to carry out *in situ* IR spectroscopy.

2.2. Catalyst characterization

2.2.1. Inductively coupled plasma optical emission spectroscopy (ICP-OES)

The elemental composition of Raney-Fe was determined by ICP-OES analysis on a Spectroblue spectrophotometer of AMETEK Inc. Typically, 25 mg sample was dissolved in 10 ml concentrated HCl. The mixture was heated until the sample was fully dissolved. Samples were measured in duplo against a standard curve. The Fe content of the Raney-Fe material was 85 wt%. This value was used to determine the C/Fe ratio of carburized samples. The Al content was 4 wt%, the remained being attributed to O, most likely in the form of residual aluminum (hydr)oxides and surface Fe-oxide due to passivation.

2.2.2. Transmission electron microscopy (TEM)

A few milligrams of catalyst powder were suspended in ethanol. The suspension was sonicated to fully suspend all particles. Afterwards, a few drops of the suspension were applied on a carbon-coated copper grid. TEM images were captured using a FEI Technai 20 transmission electron microscope using an acceleration voltage of 200 kV with a LaB6 filament. ImageJ was used to process the images and determine the average particle size.

2.2.3. In situ IR spectroscopy

Infrared spectroscopy was carried out on a Bruker Vertex 70v spectrometer equipped with DTGS detector by averaging 8 spectra at a 2 cm^{-1} resolution. IR spectra were recorded in a controlled environment cell with CaF_2 windows. Typically, the samples were pressed into self-supporting wafers of ca. 10 mg. *In situ* reduction of the Raney-Fe sample required slightly milder conditions (50/50 vol% H_2/N_2, 430 °C, 1 h, 1 bar) in comparison with Fe/SiO_2 (50/50 vol% H_2/N_2, 550 °C, 6 h, 1 bar). After reduction, the sample was outgassed (250 °C, 10 min) and the cell was cooled to about −170 °C using liquid N_2. Then, CO was dosed to the cell in small increments. After a CO pressure of 50 mbar was reached, a background IR spectrum was recorded followed by a slow increase of the temperature of the sample by halting the cooling. IR spectra were recorded every 10 °C.

2.2.4. Quasi in situ X-ray photoelectron spectroscopy (XPS)

XPS spectra were recorded in a Kratos AXIS Ultra 600 spectrometer equipped with a monochromatic Al K_α X-ray source (hv = 1486.6 eV). Region scans were recorded at a pass energy of 40 eV (step size 0.1 eV) and survey scans were recorded at a pass energy of 160 eV (step size 0.5 eV) with the background pressure kept below 5×10^{-9} mbar. A high-temperature reaction cell (Kratos, WX-530) was used to pretreat the sample, which was pressed into a pellet placed on a stainless-steel stub. This allowed *in vacuo* sample transfer into the XPS analysis chamber. Reduction was performed in a 100% H_2 flow (50 ml/min, at 1 bar) at atmospheric pressure at 550 °C for 12 h (heating rate 5 °C/min). After reduction, the sample was cooled to 30 °C or 250 °C. Syngas (16% H_2 and 8% CO in Ar, 50 ml/min, 1 bar) or CO (8% CO in Ar, 50 ml/min, 1 bar) was used for carburization. After a certain time, the reaction was stopped and the sample was transferred to the XPS analysis chamber after evacuation. Fitting of the XPS spectra was done using Voigt functions after a Shirley background subtraction using the CasaXPS software (2.3.18PR1.0).

2.2.5. In situ X-ray diffraction (XRD)

XRD was carried out on a Rigaku D/max-2600/PC apparatus equipped with a D/teX ultrahigh-speed detector and scintillation counter. The X-ray generator consisted of a Cu rotating anode target with a maximum power of 9 kW. All the tests were operated at 40 mA and 40 kV. *In situ* XRD patterns were recorded in an Anton Paar XRK-900 cell equipped with a CO/H_2/inert gas inlet system.

2.2.6. In situ Mössbauer spectroscopy

Transmission ^{57}Fe Mössbauer spectra were collected at 120 K and 300 K with a sinusoidal velocity spectrometer using a ^{57}Co (Rh) source. Velocity calibration was carried out using an α-Fe foil at room temperature. The source and the absorbing samples were kept at the same temperature during the measurements. The Mössbauer spectra were fitted using the Mosswinn 4.0 software. Carburization experiments were performed in a state-of-the-art high-pressure Mössbauer *in situ* cell. The high-pressure beryllium windows used in this cell contain 0.08% Fe, whose spectral contribution was fitted and removed from the final spectra.

2.3. Pre-treatment

In each experiment, 50 mg catalyst precursor was loaded in a quartz tubular flow reactor. The gas feed was controlled by thermal mass flow controllers. The effluent mixture was analyzed using an online mass spectrometer (MS, Balzers TPG-300) and an online gas chromatograph (GC, Compact GC 4.0). Samples were first reduced in a diluted H_2 flow (20% H_2 in Ar, 50 ml/min, 1 bar) at 430 °C using a rate of 5 °C/min followed by a dwell of 1 h. After reduction, the reactor was cooled in Ar to the temperature for investigation of the influence of temperature, duration and gas-phase composition on the carburization process.

A first set of experiments involved carburization in syngas (16% H_2 and 8% CO in Ar, 50 ml/min) or CO (8% CO in Ar, 50 ml/min) at 1 bar for 40 min at varying temperatures. The second set of carburization experiments were carried out either in syngas (16% H_2 and 8% CO in Ar, 50 ml/min) or CO (8% CO in Ar, 50 ml/min) at 1 bar and 250 °C for varying durations. In a third set of experiments, carburization was done in syngas with varying H_2/CO ratio ((0–64) % H_2 and 8% CO in Ar, 50 ml/min) at 1 bar and 250 °C for 40 min. After carburization, the catalyst was flushed in Ar and cooled to room temperature. TPH experiments were then conducted by heating the reactor to 750 °C at a rate of 5 °C/min in diluted H_2 flow (20% H_2 in Ar, 50 ml/min). During TPH, the main hydrocarbon product was CH_4 (>96%), which was followed by online MS. To quantitatively determine the CH_4 flow rate, the reactor effluent was analyzed by an online GC at regular intervals. The amount of released C atoms was calculated by integrating the CH_4 flow during the experiment.

2.4. Carburization kinetics

The kinetics of the carburization process were followed in a steady-state isotopic transient kinetic analysis (SSITKA) setup. Details of this setup can be found in the literature [27]. For each catalytic test, 50 mg Raney Fe mixed with SiC was loaded into the reactor and reduced in a diluted H_2 flow (20% H_2 in Ar, 50 ml/min) at 430 °C (with a ramping rate 5 °C/min) and 1.5 bar for 1 h. After reduction, the reactor was cooled to the targeted temperature (210, 230, 250, or 270 °C). H_2 was removed by flushing the catalyst bed for an additional 15 min. The carburization experiments were performed by switching from the inert Ne gas (6 + x ml/min) to a H_2/CO/Ar mixture (x/4/2 ml/min), in which x was either 0, 2, 8, or 16 ml/min. Ar was added to balance the total flow to 50 ml/min. During carburization, the transient response of CO (m/z = 28), CO_2 (m/z = 44), CH_4 (m/z = 15), H_2 (m/z = 2), H_2O (m/z = 18), Ne (m/z = 22), and Ar (m/z = 40) were monitored by online MS (ESS Catalysys). The catalytic activity was determined by online GC (Thermo Scientific Trace 1300, extended with Trace 1310 auxiliary oven). A combination of a MXT-QBond column (60 m · 0.53 mm) with a thermal conductivity detector was used to determine the concentrations of CO_2, CO, H_2 and CH_4, while a combination of a Rt-SilicaBond column (60 m · 0.32 mm) with a flame ionization detector was used to analyze hydrocarbons. The total amounts of CO effluent (unreacted), CO_2 and C_xH_y were calculated by integrating their flow during the experiment. The CO consumption amount was calculated by subtracting the total CO amount in a blank experiment with the unreacted CO amount. The total amount of H_2O was based on the O balance. After carburization, the catalyst was flushed in Ar and cooled to room temperature for TPH measurements. The procedure to quantify the amount of C atoms was similar as described above for TPH. The activation energy of carbide formation, CO_2 formation, H_2O formation, C_xH_y formation and CO consumption were determined based on their averaged formation or consumption rate in 40 min.

3. Results and discussion

As metallic Fe is typically carburized by CO, *in situ* IR spectroscopy was used to investigate the interaction of metallic Fe with CO. Fig. 1 shows the evolution of IR spectra of reduced Fe/SiO_2 upon exposure to CO at liquid N_2 temperature followed by a slow increase of the temperature. A corresponding experiment conducted on reduced Raney-Fe gave comparable results, however with a significantly lower signal-to-noise ratio due to the low transmission through this sample (Fig. S1 in ESI). A prominent band appearing in the range of 2200–2100 cm^{-1} in Fig. 1 can be ascribed to overlapping contributions of CO physisorbed on the surface and gaseous CO. During heating, CO_2 is formed at −150 °C as follows from the appearance of the IR band at 2340 cm^{-1}. CO_2 can be formed through the Boudouard reaction ($2\,CO \rightarrow C + CO_2$) on metallic Fe [28], which will result in poisoning of the Fe surface by C atoms. The CO_2 IR band shows a maximum intensity at −130 °C, which can be explained by the desorption of CO_2 at higher temperatures. The absence of features due to chemisorbed CO at these low temperatures and the formation of CO_2 indicates that CO rapidly dissociates on metallic Fe. Only at a temperature of −20 °C, a weak IR band in the range of 2000–2050 cm^{-1} is observed, which can be assigned to linear CO adsorption on Fe

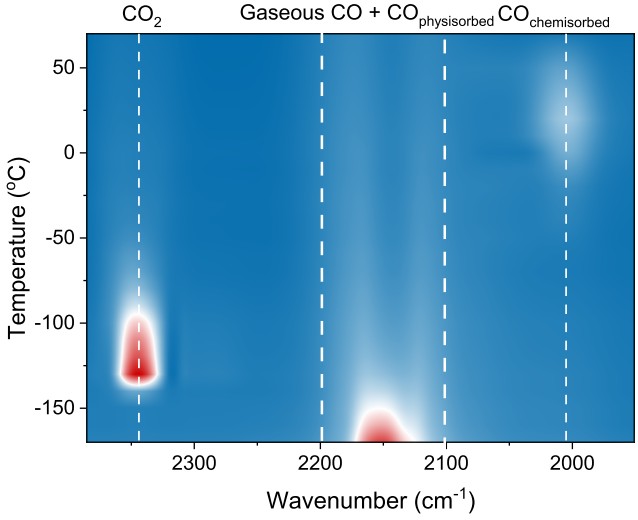

Fig. 1. *In situ* IR spectroscopy of CO adsorbed on reduced Fe/SiO_2 during heating from −170 °C to 70 °C.

[29]. A further increase of the temperature results in a lower intensity of this IR band. These data show that CO dissociation occurs very fast on metallic Fe. Part of the O atoms are released as CO_2, while the remaining C and O atoms on the surface will delay CO dissociation. Their presence is also evident due to the higher wavenumber of the IR band of adsorbed CO in the presence of co-adsorbates, which is due to lateral CO-C and CO-O interactions [30].

Additional evidence of facile CO dissociation on metallic Fe at low temperature was obtained by *quasi in situ* XPS (Fig. 2). The XPS spectrum of reduced Raney Fe was used as a reference, as there was practically no C present on the surface. The Fe 2p spectrum shows that a small fraction of Fe remains in the oxidized state, which is due to the difficulty in removing all O atoms from Raney Fe, even at a high reduction temperature of 550 °C. CO adsorption on Fe^{2+} is much weaker than on Fe^0 [31]. Upon introduction of CO at room temperature for 15 min, a weak C 1 s peak at ~284.8 eV appears, which can be attributed to sp^3 and sp^2 amorphous carbon species [32]. Prolonging CO exposure leads to a slight increase of this C signal and the formation of Fe^{2+} due to the oxidation of Fe^0. Although the XPS spectra do not contain the typical C 1 s feature of Fe-carbide at ~ 283 eV [33], its presence in very small amounts cannot be excluded given the very low overall C 1 s intensity. Nevertheless, the current data indicate that the C atoms derived from CO dissociation remain at the surface and do not diffuse into the Fe lattice under these conditions. Thus, at relatively low temperatures C can already be deposited on metallic Fe by CO dissociation and CO_2 is formed by recombination of CO with O atoms.

We next investigated the influence of temperature on the carburization process, which is determining the rate of C diffusion from the surface into the Fe lattice. For this purpose, temperature-programmed reaction (TPR) experiments in a CO atmosphere on reduced Raney-Fe were performed (Fig. 3). As CO_2 is formed by the Boudouard reaction, the evolution of CO_2 is a suitable indicator of C accumulation. It shows that CO_2 formation readily occurs at 30 °C, directly after CO is introduced. The CO_2 profile shows a maximum in this isothermal regime consistent with the notion that C remains on the surface and blocks sites for CO dissociation. Upon ramping the temperature to 175 °C, it can be seen that CO_2 formation increases in an exponential manner. This can be explained by the diffusion of C atoms from the surface to the bulk of Fe, freeing surface sites for further CO dissociation. It has been mentioned that the deformation energy needed to release the structural strain gives rise to the diffusion barrier for Fe-carbide formation [13].

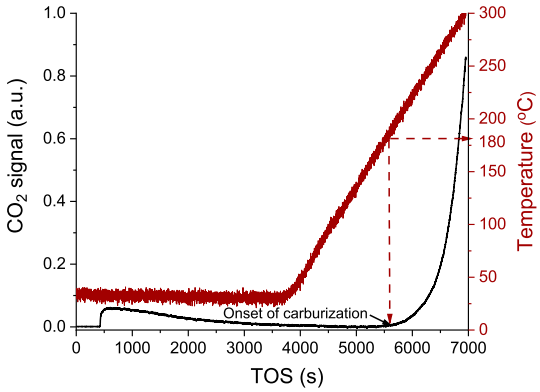

Fig. 3. CO-TPR on reduced Raney-Fe (8% CO in Ar, 50 ml/min).

Next, TPH was employed to determine the amount of C present in the catalyst after carburization of Raney-Fe in CO. First, the carburization in CO for 40 min at different temperatures was studied (Fig. 4a). CH_4 is the main product of TPH with minor amounts of other hydrocarbons as by-products. The TPH profiles obtained for samples carburized below 190 °C only show a weak broad CH_4 feature at temperatures between 200 °C and 350 °C, which can be attributed to the hydrogenation of surface C. The maximum of this feature shifts to higher temperature with increasing carburization temperature, suggesting that the C phase at the surface becomes more difficult to reduce. Upon carburization at 190 °C, the amount of CH_4 is substantially higher than at lower carburization temperatures, which indicates the onset of Fe-carbide formation. When the carburization temperature is increased, the CH_4 peak shifts to higher temperatures and increases. The shift to higher temperature can be ascribed to the lower reactivity of C atoms in Fe-carbide than C atoms at the surface [34]. The presence of a high-temperature feature after carburization at 350 °C can be explained by graphite, which can only be hydrogenated at relatively high temperature [35]. Moreover, graphite will also impede the accessibility of the Fe-carbide surface, lowering the hydrogenation of bulk C atoms [36]. This can explain the significant shift to higher temperatures of the bulk reduction feature. Fig. 4c shows the atomic C/Fe ratio obtained by integration of these TPH profiles. Consistent with CO-TPR, a low carburization temperature (35–170 °C) results in the deposition of a very small amount of C. Based on the average particle size and dispersion of the Raney-Fe catalyst of 29 nm and 3.5%, respectively (Fig. S2), the C/Fe ratio (~0.03) suggests that a monolayer coverage of C is reached. It is also consistent with

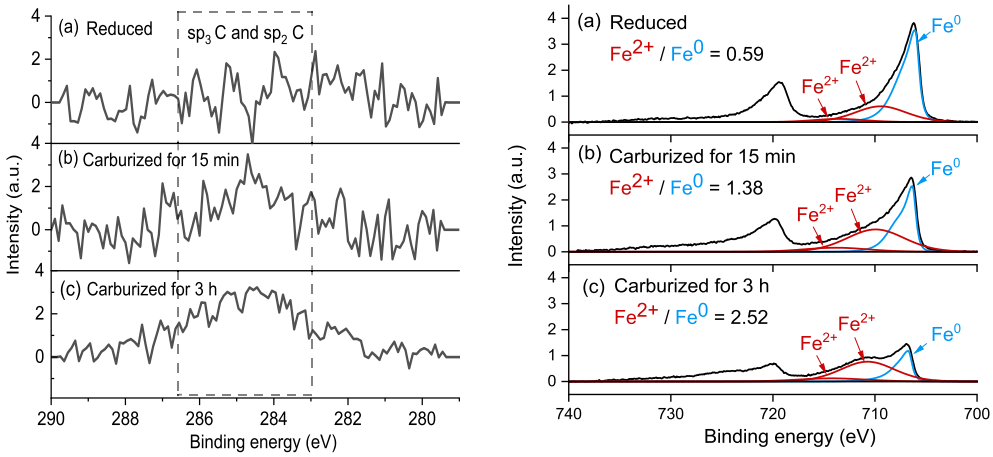

Fig. 2. XPS spectra of C 1 s region and Fe 2p after (a) reduction, (b) carburization with CO for 15 min at 25 °C, (c) carburization with CO for 3 h at 25 °C.

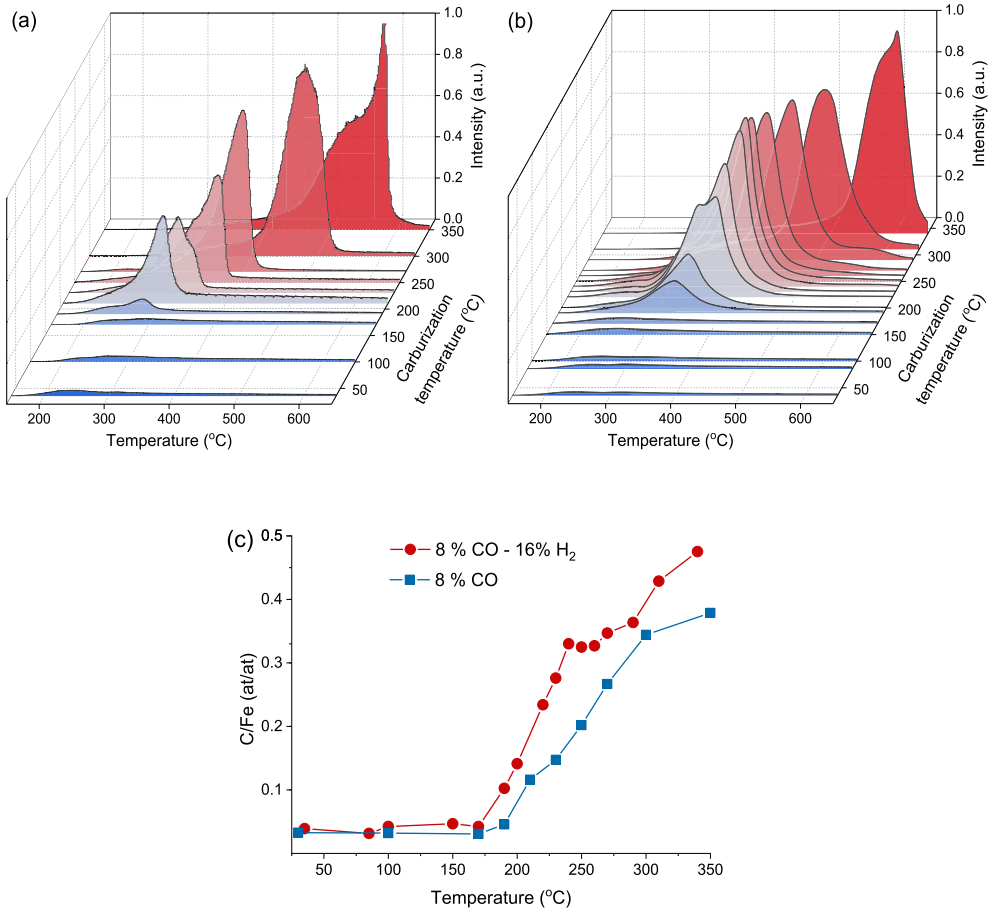

Fig. 4. TPH of carburized Raney-Fe at different carburization temperature: (a) after carburization in CO, (b) after carburization in H_2/CO = 2, and (c) the C/Fe ratio based on integration of the CH_4 signal. The carburization time was 40 min.

previous XPS data (Fig. 2) that C atoms deposited at 25 °C remain at the surface and do not diffuse into the Fe lattice. When the temperature exceeds 170 °C, deposited C can easily enter the Fe lattice and the C/Fe ratio increases with increasing carburization temperature. The TPH method allows determining the carburization degree in a facile manner.

As in practice carburization is carried out in synthesis gas mixtures, the influence of temperature on the carburization process in the presence of H_2 was also investigated (Fig. 4b). Comparison of the TPH profiles recorded with and without H_2 shows that carburization at intermediate temperatures (190–300 °C) results in more CH_4. This shows that H_2 facilitates the carburization process. The carburization rate will depend on the concentration gradient of carbon [37]. As the presence of H_2 in the gas phase will not influence the diffusion rate of C in bulk Fe, the positive effect of H_2 on the carburization kinetics can be ascribed to a higher C coverage. Similar findings have been reported earlier [14,38]. Fig. 4c shows that the presence of H_2 accelerates the formation of Fe-carbide.

The positive effect of H_2 on Fe carburization was also investigated by varying the H_2/CO ratio using a carburization time of 40 min and a temperature of 250 °C. The results in Fig. S3 show that more C diffuses into the Fe lattice with increasing H_2/CO ratio. Niemantsverdriet et al. proposed that there is competition between C diffusion into the Fe lattice and C hydrogenation [8]. It can be expected that, with increasing H_2/CO ratio, the removal of C from the surface in the form of gaseous products becomes faster than the rate of C diffusion into the surface. As the opposite is observed in our study, the carburization process was studied in more detail below.

Fig. 5 shows the C/Fe ratio determined by TPH as a function of the carburization time for different H_2/CO ratios. During the first 40 min, the carburization rate at a H_2/CO ratio of 2 (8% CO, 16% H_2) is higher than in 8% CO. This confirms the positive effect of

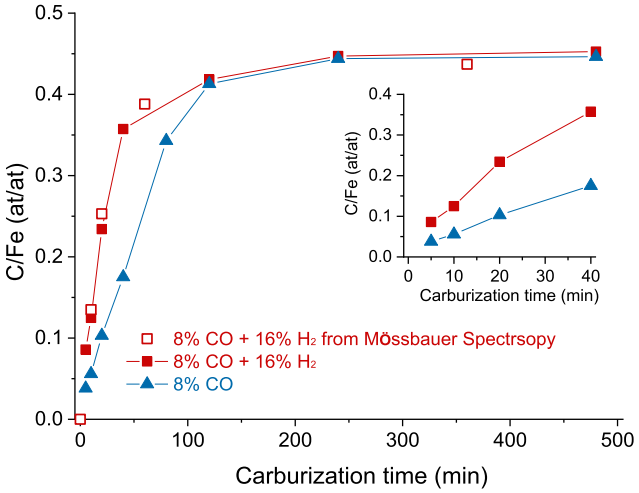

Fig. 5. C/Fe of carburized Raney-Fe as a function of carburization time under different carburization conditions at 250 °C (the inset shows a zoom of the initial 40 min).

H_2 on the carburization rate. It also explains that catalysts activated in CO need a longer induction time than those activated in syngas [39]. *In situ* Mössbauer spectra during carburization were also recorded at a H_2/CO ratio of 2. The corresponding spectra and the results of spectra deconvolution are given in Fig. S4 and Table S1, respectively. The thereof derived C/Fe ratios are added to Fig. 5. These *in situ* Mössbauer results are in good agreement with the TPH data.

In situ techniques are best equipped to study gas phase-solid phase reactions. Therefore *in situ* XRD and *in situ* Mössbauer spectroscopy were applied here to investigate closely the positive effect of H_2 on Fe carburization. *In situ* XRD shows that, after reduction and before carburization, the catalyst is completely reduced as only the typical reflections of α-Fe can be observed (Fig. 6). This is confirmed by *in situ* Mössbauer spectra, which only shows a spectral contribution of pure Fe^0 (Fig. S4, Table S1).

In pure CO, *in situ* XRD patterns recorded with increasing temperature show that carburization starts at 220 °C. At this temperature, new reflections due to χ-Fe_5C_2 appear (Fig. 6a). Thermodynamically, the formation of ε(′)-carbide is favored at low temperature and low H_2/CO ratio [13]. The observation of χ-Fe_5C_2 instead of ε(′)-carbide can be an indication of a kinetic limitation, leading to the formation of the Fe-carbide with a lower C/Fe ratio. When synthesis gas (H_2/CO = 2) is used, carburization proceeds differently (Fig. 6b). Metallic Fe is converted into Fe-carbide at a lower temperature and ε(′)-carbide becomes the dominant Fe-carbide phase. Above 320 °C, ε(′)-carbide transforms to χ-Fe_5C_2 and the latter becomes the main Fe-carbide phase at higher temperatures, because ε(′)-carbide formation is entropically not favored [13]. Above 380 °C, χ-Fe_5C_2 transforms to *Θ*-Fe_3C, which is expected at high temperature [40]. Haglund *et al.* reported that *Θ*-Fe_3C has a metallic character and is susceptible to the buildup of surface C species [41]. It has indeed been reported that *Θ*-Fe_3C formation is typically accompanied by graphite growth [13,25,42]. This can explain the relatively high C/Fe ratios observed in Fig. 4c obtained after carburization at higher temperatures in a H_2/CO = 2 mixture and the asymmetric TPH peaks in Fig. 4.

De Smit *et al.* reported that the formation of ε(′)-carbides is kinetically limited by the diffusion of C atoms into α-Fe due to the higher C/Fe ratio of this phase in comparison to χ-Fe_5C_2 [13]. This can explain why ε(′)-carbides are typically formed in catalysts containing small Fe particles [43] or having a structure with an expanded lattice obtained during rapid quenching of Fe [9]. The pretreatment conditions have a pronounced effect on the carbide phase formed upon carburization. It has been found that H_2 reduction of the Fe precursor leads to ε(′)-carbide during the FT reaction, while reduction in CO or syngas preferentially results in χ-Fe_5C_2 formation [44]. Our observations show that the presence of H_2 in the carburizing gas mixture enhances the rate of carburization, which may account for the formation of the carbon-richer ε(′)-carbide phase.

Additional *in situ* Mössbauer spectroscopy measurements were carried out to understand how ε(′)-carbide formation depended on the presence of H_2. As Fig. 7 shows, upon carburization without H_2, only a small amount (~22%) of a disordered Fe-carbide phase is formed. The broad signal lines do not allow accurate identification of the formed Fe-carbide. Most likely, these disordered Fe_xC species are a mixture of χ-Fe_5C_2 and ε(′)-carbide. The Mössbauer data show that Fe-oxides are absent, which can be attributed to the much lower diffusion constant of O in Fe in comparison with C [21]. The introduction of H_2 substantially increases the carburization degree. As a result, a mixture of 19% χ-Fe_5C_2 and 37% ε(′)-carbide is obtained. The higher carburization degree is consistent with the TPH results. A further increase of the H_2 partial pressure increases the total spectral contribution of the Fe-carbides. The increase is largest for ε-Fe_2C, which is in line with the above data that showed the promoting effect of H_2 on the formation of the carbon-richer ε(′)-carbide phase. At the highest H_2/CO ratio, no additional χ-Fe_5C_2 is formed and only the spectral contribution of ε(′)-carbide increases. It was also observed that carburization in a mixture of 8% CO and 16% H_2 leads to more ε(′)-carbide than carburization in 8% CO (details in Figs. S4, S5 and Table S2). These results further confirm that the presence of H_2 favors the formation of the carbon-richer ε(′)-carbide phase.

Based on the strong correlation between the carburization rate and the H_2 partial pressure, we speculate that the higher C diffusion rate is due to a higher C coverage of the surface. The underlying mechanism for this promotion remains unknown considering the complex nature of the reactions on the surface. This led us to investigate the influence of H_2 on the surface C and O coverages. The surface reactions involve many elementary reaction steps, some of which are sensitive to the H_2 partial pressure. Among them, H_2 may assist carbide formation in two ways, *i.e.*, by (i) removing O from the surface thus creating vacancies for CO dissociation [45] or (ii) enhancing CO dissociation via H-assisted CO dissociation. According to DFT calculations for the Fe(100) surface,

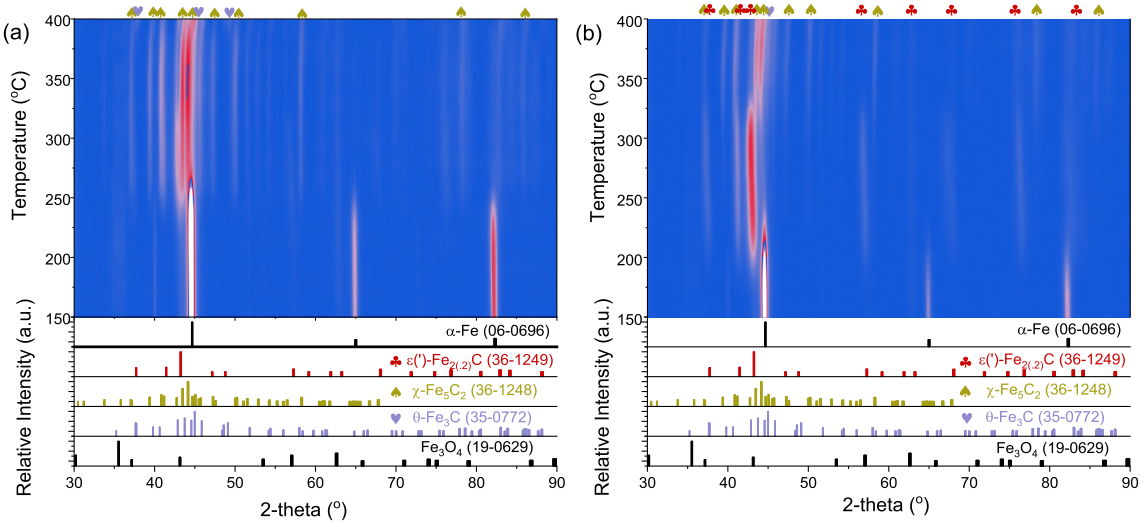

Fig. 6. *In situ* XRD patterns of carburization of reduced Raney-Fe in (a) CO (20% CO in Ar, 50 ml/min, 1 bar) and (b) H_2/CO (8% CO −16% H_2 in Ar, 50 ml/min, 1 bar).

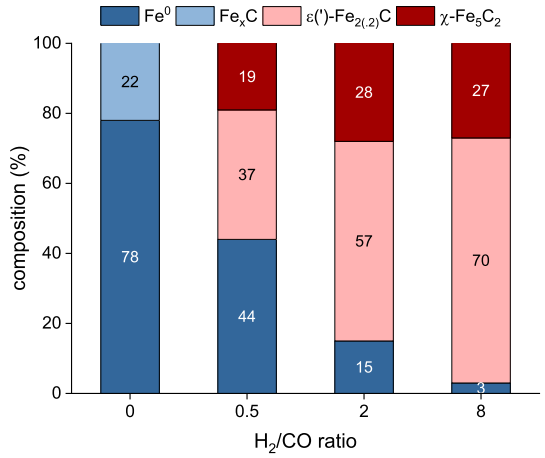

Fig. 7. Fe-carbide phase composition as a function of H_2/CO ratio after carburization at 250 °C, 1 bar for 1 h (data obtained from Mössbauer spectra shown in Fig. S5 and Table S2).

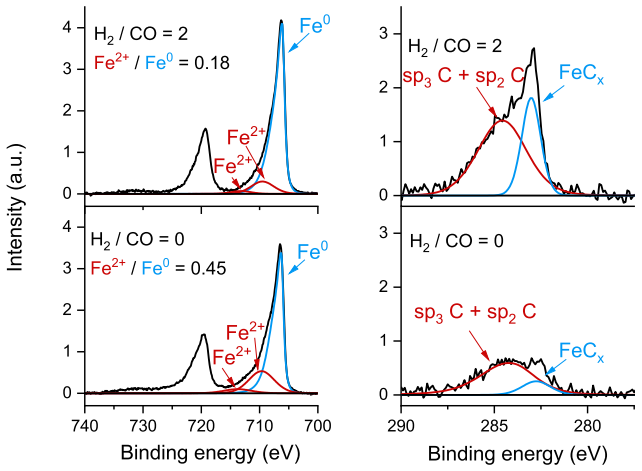

Fig. 8. XPS spectra of Fe 2p region and C 1 s region after carburization at 250 °C at 1 bar for 20 min as a function of the H_2/CO ratio.

direct CO dissociation is the preferred pathway with only a small contribution of H-assisted pathways. Only on close-packed surfaces such as Fe(1 1 0), which are less active in CO dissociation and, thus, contribute less to the total activity, H-assisted routes might also play a role [46]. In addition, Broos *et al.* reported that CO dissociation proceeds via direct C–O bond scission on the stepped sites on the Fe-carbide surface, while H-assisted CO dissociation is only preferred on surfaces with a large occupancy of subsurface C atoms [47]. As in our case carburization starts from the C-free metallic Fe surface, direct CO dissociation is expected to be the dominant pathway. As can be appreciated from Fig. 5, the C content increases nearly linearly with time on stream (TOS) during the first 40 min both in the presence and absence of H_2. During this period, the surface will gradually be covered by C. As the carburization rate hardly changes in time, it can be assumed that the mechanism of CO dissociation is not changed dramatically in the initial stage of the reaction and dominated by direct CO dissociation, which is preferred on metallic Fe and carbon-poor Fe surfaces. This conclusion is also in line with the IR results shown above, evidencing that direct CO dissociation can already occur in the absence of H_2 at sub-ambient conditions. Taken together, it is unlikely that H_2 plays an important role in CO dissociation. Therefore, it is reasonable to speculate that enhanced removal of O from the surface accelerates CO dissociation and thus carburization.

To confirm whether H_2 enhances O removal, TPH and XPS were employed to determine the bulk and surface composition as a function of the carburization conditions. In the TPH profiles, the intensities of the H_2O and CH_4 signals were used as respective indicators of the amounts of O and C left on the catalyst after carburization (Figs. S6 and S3 in the ESI). These data show that a higher H_2/CO ratio during carburization results in a lower O and a higher C content. The positive effect of H_2 on O removal can also be followed by XPS (Fig. 8). Carburization with only CO at 250 °C leads to a Fe^{2+}/Fe^0 ratio of 0.45. In the presence of H_2 (H_2/CO = 2), this ratio decreases to 0.18, indicating a lower extent of oxidation. The more metallic nature of the surface in the presence of H_2 goes in parallel with a higher C 1 s signal. The C 1 s binding energy of the Fe-carbide at 283.1 eV did not vary with the C/Fe ratio. These data indicate that H_2 leads to an increased rate of O removal and a higher C coverage. The higher C coverage implies a larger driving force for C diffusion into bulk Fe, which can explain the higher carburization rate observed with increasing H_2 pressure. This fits with near-ambient-pressure XPS results that indicated that O atoms derived from CO dissociation can block part of the Fe surface and decrease C diffusion into bulk Fe [48]. A recent report mentioned that pre-deposited C on metallic Fe preferentially leads to ε(́)-carbide formation [19]. This agrees with the finding that a higher C coverage due to the presence of H_2, leads to formation of ε(́)-carbide instead of χ-carbide (Fig. 7).

To better understand the effect of H_2 on the carburization kinetics, additional experiments with varying carburization temperature and H_2/CO ratio were performed. Fig. 9 shows Arrhenius plots for the carburization reaction as a function of the H_2/CO ratio. In the absence of H_2 (H_2/CO = 0), CO_2 formation is the only pathway for O removal. The similar apparent activation energies of CO_2 formation and carburization (78 and 79 kJ/mol, respectively) suggest that these reactions share the same rate-limiting step. Removal of O is a likely candidate for the rate-limiting step. In the presence of H_2, O is expected to be removed faster [49]. This is experimentally reflected by the decrease of the apparent activation energy for carburization. The value ranges between 28 and 34 kJ/mol depending on the H_2/CO ratio. These values are close to the apparent activation energy for H_2O formation (31–33 kJ/mol), suggesting that under these conditions H_2O formation is the rate-controlling step in the overall carburization process. The slower removal of O via CO_2 formation as compared to H_2O is in line with DFT calculations, which showed that the activation energy for O removal via H_2O formation is significantly lower than via CO_2 formation. Since that the apparent activation energies for carburization are in the same range as the activation energy for O removal independent of the presence of H_2, it can be inferred that O removal is likely limiting the overall carburization process. As furthermore O removal via H_2O is easier than via CO_2, H_2 can accelerate the carburization of Fe.

Hydrocarbons were observed in the effluent stream already during carburization. Thus, there is competition for surface C intermediates between hydrocarbon formation and carburization [37]. Comparison of the measured apparent activation energies for these two reactions (Fig. 9a and 9d) shows that hydrocarbon formation is much more difficult than carburization. In line width his, the overall activation energy for CO consumption is close to the averaged apparent activation energies for carburization and hydrocarbons formation. In the presence of H_2, the apparent activation energy for H_2O removal is lower than that of hydrocarbon formation under all conditions. Hence, it can be concluded that the predominant role of H_2 is the removal of O and not of C. In summary, increasing the H_2 partial pressure results in faster removal of O, freeing vacancies needed for CO dissociation. This results in a higher C coverage,

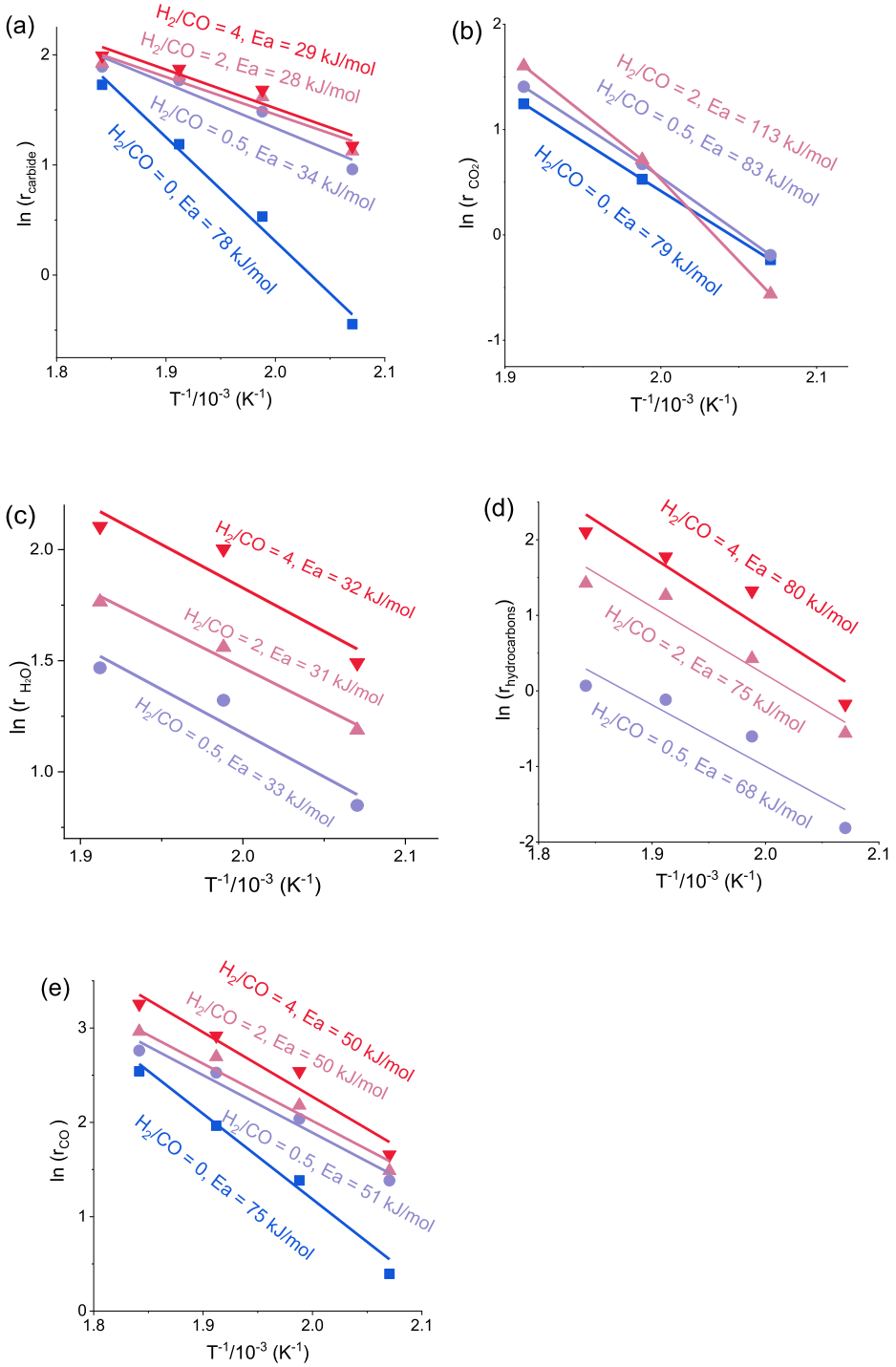

Fig. 9. Kinetic parameters derived from carburization during 40 min at different H_2/CO ratios: (a) accumulation of C in bulk Fe, (b) CO_2 formation, (c) H_2O formation, (d) hydrocarbon formation, and (e) CO consumption.

benefiting the rate of carburization. This is in accordance with the results obtained by *in situ* XRD and Mössbauer spectroscopy.

4. Conclusions

The mechanism of the carburization of Raney Fe used as a model for carburization of Fe-based FT catalysts was investigated by spectroscopic and temperature-programmed techniques. Carburization of reduced Fe can be divided into two stages: C deposition on the surface and C diffusion into the Fe bulk. *In situ* IR spectroscopy of adsorbed CO verified the high reactivity of metallic Fe towards CO dissociation. Under such conditions, O can be removed as CO_2 and C atoms remain on the surface of reduced Fe. CO-TPR and TPH indicate that the temperature for overcoming the barrier for C diffusion into the Fe lattice is about 180 °C. The Fe-carbide phase and the rate of its formation depends on the temperature and the composition of the carburizing gas. While at low H_2/CO ratio χ-carbide is formed, ε'()-carbide is dominant at higher H_2/CO ratio as determined by *in situ* XRD and Mössbauer spectroscopy.

H_2 increases the rate of carburization rate, because it accelerated the removal of O via H_2O (as opposed to CO_2), regenerating surface vacancies for CO dissociation and thus providing a higher C coverage. The rate of carburization is much faster than the rates of surface hydrogenation reactions of C into hydrocarbons in the early stage of carburization. Intrinsically, all these phenomena stem from the strong Fe-C bond and the low C diffusion barrier. This work sheds light on how bulk C diffusion is affected by surface reactions and how ε(́)-carbide or χ-carbide can be formed by adjusting the carburization conditions.

Declaration of Competing Interest

The authors declare that they have no known competing financial interests or personal relationships that could have appeared to influence the work reported in this paper.

Acknowledgements

Jiachun Chai acknowledges financial support of the China Scholarship Council. This work was supported by the National Key Research and Development Program of China (no. 2017YFB0602500). The authors thank Adelheid Elemans-Mehring of Eindhoven University of Technology for elemental analysis.

Appendix A. Supplementary data

Supplementary data to this article can be found online at https://doi.org/10.1016/j.jcat.2021.05.027.

References

[1] J. Li, Y. He, L. Tan, P. Zhang, X. Peng, A. Oruganti, G. Yang, H. Abe, Y. Wang, N. Tsubaki, Integrated Tunable Synthesis of Liquid Fuels via Fischer-Tropsch Technology, Nat. Catal. 1 (2018) 787–793.
[2] J. Sun, G. Yang, X. Peng, J. Kang, J. Wu, G. Liu, N. Tsubaki, Fischer-Tropsch Synthesis for Non-Automotive Applications, ChemCatChem 11 (2019) 1412–1424.
[3] P.H.J. Cheng, P. Ellis, S. French, G. Kelly, C.M. Lok, Density Functional Theory Study of Iron and Cobalt Carbides for Fischer-Tropsch Synthesis, J. Phys. Chem. C 114 (2010) 1085–1093.
[4] H.M. Torres Galvis, J.H. Bitter, T. Davidian, M. Ruitenbeek, A.I. Dugulan, K.P. de Jong, Iron Particle Size Effects for Direct Production of Lower Olefins from Synthesis Gas, J. Am. Chem. Soc. 134 (2012) 16207–16215.
[5] J.Y. Park, Y.J. Lee, P.K. Khanna, K.W. Jun, J.W. Bae, Y.H. Kim, Alumina-Supported Iron Oxide Nanoparticles as Fischer-Tropsch Catalysts: Effect of Particle Size of Iron Oxide, J. Mol. Catal. A Chem. 323 (2010) 84–90.
[6] V.P. Santos, T.A. Wezendonk, J.J. Jaen, A.I. Dugulan, M.A. Nasalevich, H.U. Islam, A. Chojecki, S. Sartipi, X. Sun, A.A. Hakeem, A.C. Koeken, M. Ruitenbeek, T. Davidian, G.R. Meima, G. Sankar, F. Kapteijn, M. Makkee, J. Gascon, Metal Organic Framework-Mediated Synthesis of Highly Active and Stable Fischer-Tropsch Catalysts, Nat. Commun. 6 (2015) 6451.
[7] P. Thüne, P. Moodley, F. Scheijen, H. Fredriksson, R. Lancee, J. Kropf, J. Miller, J. W. Niemantsverdriet, The Effect of Water on the Stability of Iron Oxide and Iron Carbide Nanoparticles in Hydrogen and Syngas Followed by *in situ* X-ray Absorption Spectroscopy, J. Phys. Chem. C 116 (2012) 7367–7373.
[8] J.W. Niemantsverdriet, A.M. Van Der Kraan, On the Time-Dependent Behavior of Iron Catalysts in Fischer-Tropsch Synthesis, J. Catal. 72 (1981) 385–388.
[9] K. Xu, B. Sun, J. Lin, W. Wen, Y. Pei, S. Yan, M. Qiao, X. Zhang, B. Zong, Epsilon-Iron Carbide as a Low-Temperature Fischer-Tropsch Synthesis Catalyst, Nat. Commun. 5 (2014) 5783.
[10] G. Le Caer, J.M. Dubois, M. Pijolat, V. Perrlchon, P. Busslere, Characterization by Mössbauer Spectroscopy of Iron Carbides Formed by Fischer-Tropsch Synthesis, J. Phys. Chem. B 86 (1982) 4799–4808.
[11] X.W. Liu, Z. Cao, S. Zhao, R. Gao, Y. Meng, J.X. Zhu, C. Rogers, C.F. Huo, Y. Yang, Y.W. Li, X.D. Wen, Iron Carbides in Fischer-Tropsch Synthesis: Theoretical and Experimental Understanding in Epsilon-Iron Carbide Phase Assignment, J. Phys. Chem. C 121 (2017) 21390–21396.
[12] Q. Chang, C. Zhang, C. Liu, Y. Wei, A.V. Cheruvathur, A.I. Dugulan, J.W. Niemantsverdriet, X. Liu, Y. He, M. Qing, L. Zheng, Y. Yun, Y. Yang, Y. Li, Relationship between Iron Carbide Phases (ε-Fe_2C, Fe_7C_3, and χ-Fe_5C_2) and Catalytic Performances of Fe/SiO_2 Fischer-Tropsch Catalysts, ACS Catal. 8 (2018) 3304–3316.
[13] E. de Smit, F. Cinquini, A.M. Beale, O.V. Safonova, W. van Beek, P. Sautet, B.M. Weckhuysen, Stability and Reactivity of ε-χ-θ Iron Carbide Catalyst Phases in Fischer-Tropsch Synthesis: Controlling μ_C, J. Am. Chem. Soc. 132 (2010) 14928–14941.
[14] L. Niu, X. Liu, J. Liu, X. Liu, X. Wen, Y. Yang, J. Xu, Y. Li, Tuning Carburization Behaviors of Metallic Iron Catalysts with Potassium Promoter and CO/syngas/C_2H_4/C_2H_2 gases, J. Catal. 371 (2019) 333–345.
[15] R. Asano, Y. Sasaki, K. Ishii, Carburization of Iron by Ar–CO–H_2 at 1523 K, ISIJ Int. 42 (2001) 121–126.
[16] H. Kim, D.J. Min, S.M. Jung, A Kinetic Study on Carburization of Fe by Using ^{13}CO Isotope Gas, ISIJ Int. 53 (2013) 199–206.
[17] A. Schneider, G. Inden, Carbon Diffusion in Cementite (Fe_3C) and Hägg Carbide (Fe_5C_2), Calphad 31 (2007) 141–147.
[18] V.L. de la Concepción, H.N. Lorusso, H.G. Svoboda, Effect of Carbon Content on Microstructure and Mechanical Properties of Dual Phase Steels, Procedia Mater. Sci. 8 (2015) 1047–1056.
[19] P. Wang, W. Chen, F.K. Chiang, A.I. Dugulan, Y. Song, R. Pestman, K. Zhang, J. Yao, B. Feng, P. Miao, W. Xu, E.J.M. Hensen, Synthesis of Stable and Low-CO_2 Selective ε-Iron Carbide Fischer-Tropsch Catalysts, Sci. Adv. 4 (2018) eaau2947.
[20] W. Chen, Z. Fan, X. Pan, X. Bao, Effect of Confinement in Carbon Nanotubes on the Activity of Fischer-Tropsch Iron Catalyst, J. Am. Chem. Soc. 130 (2008) 9414–9419.
[21] A. Bramely, F.W. Haywood, A.T. Cooper, J.T. Watts, the Diffusion of Non-metallic Elements, Trans. Faraday Soc. 31 (1934) 707–734.
[22] G.B. Raupp, W.N. Delgass, Mikbauer Investigation of Supported Fe Catalysts III: *in situ* Kinetics and Spectroscopy during Fischer-Tropsch Synthesis, J. Catal. 58 (1979) 361–369.
[23] L. Niu, X. Liu, X. Liu, Z. Lv, C. Zhang, X. Wen, Y. Yang, Y. Li, J. Xu, *In situ* XRD Study on Promotional Effect of Potassium on Carburization of Spray-Dried Precipitated Fe_2O_3 Catalysts, ChemCatChem 9 (2017) 1691–1700.
[24] E. De Grave, A. Van Alboom, Evaluation of Ferrous and Ferric Miissbauer Fractions, Phys. Chem. Miner. 18 (1991) 337–342.
[25] Local and Long Range Order in Promoted Iron-based Fischer–Tropsch Catalysts: A Combined in situ X-ray Absorption Spectroscopy/Wide Angle X-ray Scattering Study, J. Catal. 262 (2009), 244–256
[26] S. Li, G.D. Meitzner, E. Iglesia, Structure and Site Evolution of Iron Oxide Catalyst Precursors during the Fischer-Tropsch Synthesis, J. Phys. Chem. B 105 (2001) 5743–5750.
[27] W. Chen, R. Pestman, B. Zijlstra, I.A.W. Filot, E.J.M. Hensen, Mechanism of Cobalt-Catalyzed CO Hydrogenation: 1. Methanation, ACS Catal. 7 (2017) 8050–8060.
[28] S. Zhao, X. Liu, C. Huo, Y. Li, J. Wang, H. Jiao, Determining Surface Structure and Stability of ε-Fe_2C, χ-Fe_5C_2, θ-Fe_3C and Fe_4C Phases under Carburization Environment from Combined DFT and Atomistic Thermodynamic Studies, Catal. Struct. React. 1 (2014) 44–60.
[29] E. Boellaard, A.M. van der Kraan, J.W. Geus, Preparation, Reduction, and CO Chemisorption Properties of a Cyanide-derived Fe/Al_2O_3 Catalyst, Appl. Catal. A 147 (1996) 207–227.
[30] A.F.H. Wielers, A.J.H.M. Kock, C.E.C.A. Hop, J.W. Geus, A.M. van der Kraan, The Reduction Behavior of Silica-Supported Iron Catalysts: A Mossbauer and Infrared Spectroscopic and Alumina-Supported Study, J. Catal. 117 (1989) 1–18.
[31] J. Diaz, G. Paolicelli, S. Ferrer, F. Comin, Heats of Adsorption of Linear CO Species Adsorbed on Reduced Fe/Al_2O_3 Catalysts Using the AEIR Method in Diffuse Reflectance Mode, Phys. Rev. B 54 (1996) 8064–8069.
[32] Z. Yang, T. Zhao, X. Huang, X. Chu, T. Tang, Y. Ju, Q. Wang, Y. Hou, S. Gao, Modulating the Phases of Iron Carbide Nanoparticles: from a Perspective of Interfering with the Carbon Penetration of Fe@Fe_3O_4 by Selectively Adsorbed Halide Ions, Chem. Sci. 8 (2017) 473–481.
[33] A. Wiltner, Ch. Linsmeier, Formation of Endothermic Carbides on Iron and Nickle, Phys. Stat. Sol. 5 (2004) 881–887.
[34] S.A. Eliason, C.H. Bartholomew, Temperature-Programmed Reaction Study of Carbon Transformations on Iron Fischer-Tropsch Catalysts During Steady-State Synthesis, Stud. Surf. Sci. Catal. 111 (1997) 517–526.
[35] J. Xu, C.H. Bartholomew, Temperature-Programmed Hydrogenation (TPH) and *in Situ* Mossbauer Spectroscopy Studies of Carbonaceous Species on Silica-Supported Iron Fischer-Tropsch Catalysts, J. Phys. Chem. B 109 (2005) 2392–2403.
[36] E. de Smit, B.M. Weckhuysen, the Renaissance of Iron-based Fischer-Tropsch Synthesis: on the Multifaceted Catalyst Deactivation Behaviour, Chem. Soc. Rev. 37 (2008) 2758–2781.
[37] P.C. Prasannan, Carburization of Steels–an Overview, Indian J. Eng. Mater. Sci. 1 (1994) 221–228.
[38] H. Arakawa, A.T. Bell, Effects of Potassium Promotion on the Activity and Selectivity of Iron Fischer-Tropsch Catalysts, Ind. Eng. Chem. Process Des. Dev. 22 (1983) 97–103.
[39] L.D. Mansker, Y. Jin, D.B. Bukur, A.K. Datye, Characterization of Slurry Phase Iron Catalysts for Fischer-Tropsch Synthesis, Appl. Catal. A 186 (1999) 277–296.
[40] S. Nagakura, Study of Metallic Carbides by Electron Diffraction Part III. Iron Carbides, J. Phys. Soc. Jpn. 14 (1959) 186–195.
[41] J. Haglund, G. Grimvall, T. Jarlborg, Electronic Structure, x-ray Photoemission Spectra, and Transport Properties of Fe_3C (Cementite), Phys. Re.v B Condens. Matter 44 (1991) 2914–2919.
[42] A.N. Pour, M.R. Housaindokht, S.F. Tayyari, J. Zarkesh, Deactivation Studies of Nano-Structured Iron Catalyst in Fischer-Tropsch Synthesis, J. Nat. Gas Chem. 19 (2010) 333–340.

[43] J.W. Niemantsverdriet, A.M. van der Kraan, Behavior of Metallic Iron Catalysts during Fischer-Tropsch Synthesis Studied with Mossbauer Spectroscopy, X-ray Diffraction, Carbon Content Determination and Reaction Kinetic Measurements, J. Phys. Chem. B 84 (1980) 3363–3370.
[44] D.B. Bukur, K. Okabe, M.P. Rosynek, C. Li, D. Wang, K.R.P.M. Rao, G.P. Huffman, Activation Studies with a Precipitated Iron Catalyst for Fischer-Tropsch Synthesis: I. Characterization Studies, J. Catal. 155 (1995) 353–365.
[45] J.B. Butt, Carbide Phases on Iron-based Fischer-Tropsch Synthesis Catalysis Part II: some Reaction Studies, Catal. Lett. 7 (1990) 83–106.
[46] M.R. Elahifard, M.P. Jigato, J.W. Niemantsverdriet, Direct versus Hydrogen-Assisted CO Dissociation on the Fe (100) Surface: A DFT Study, ChemPhysChem 13 (2012) 89–91.
[47] R.J.P. Broos, B. Zijlstra, I.A.W. Filot, E.J.M. Hensen, Quantum-Chemical DFT Study of Direct and H- and C-Assisted CO Dissociation on the chi-Fe_5C_2 Hagg Carbide, J. Phys. Chem. C Nanomater. Interfaces 122 (2018) 9929–9938.
[48] X. Zhou, G.J.A. Mannie, J. Yin, X. Yu, C.J. Weststrate, X. Wen, K. Wu, Y. Yang, Y. Li, J.W. Niemantsverdriet, Iron Carbidization on Thin-Film Silica and Silicon: A Near-Ambient-Pressure X-ray Photoelectron Spectroscopy and Scanning Tunneling Microscopy Study, ACS Catal. 8 (2018) 7326–7333.
[49] T. Li, X. Wen, Y. Li, H. Jiao, Mechanisms of CO Activation, Surface Oxygen Removal, Surface Carbon Hydrogenation, and C-C Coupling on the Stepped Fe (710) Surface from Computation, J. Phys. Chem. C 122 (2018) 15505–15519.